processes

MDPI

Article

Development of a $CaCO_3$ Precipitation Method Using a Peptide and Microwaves Generated by a Magnetron

Fumihiro Kayamori [1,2,*], Hiroyuki Togashi [2,3], Natsumi Endo [1], Makoto Ozaki [1], Kan Hirao [1], Yonejiro Arimoto [4], Ryuji Osawa [5], Takaaki Tsuruoka [1], Takahito Imai [6], Kin-ya Tomizaki [6,7], Tomohiro Umetani [2,8], Nobuhiro Nakanishi [2,3,9] and Kenji Usui [1,2,9,*]

1 Faculty of Frontiers of Innovative Research in Science and Technology (FIRST), Konan University, Chuo-ku, Kobe 650-0047, Hyogo, Japan; tsuruoka@konan-u.ac.jp (T.T.)
2 Research Institute for Nanobio-Environment and Non-Ionizing Radiation (RINNIR), Konan University, Chuo-ku, Kobe 650-0047, Hyogo, Japan; umetani@konan-u.ac.jp (T.U.); nob-nakanishi@dspr.co.jp (N.N.)
3 DSP Research, Inc., Chuo-ku, Kobe 650-0047, Hyogo, Japan
4 Minato Medical Science Co., Ltd., Chuo-ku, Kobe 650-0047, Hyogo, Japan
5 Seikoh Giken Co., Ltd., Matsudo 270-2214, Chiba, Japan
6 Department of Materials Chemistry, Ryukoku University, Otsu 520-2194, Shiga, Japan; tomizaki@rins.ryukoku.ac.jp (K.-y.T.)
7 Innovative Materials and Processing Research Center, Ryukoku University, Otsu 520-2194, Shiga, Japan
8 Faculty of Intelligence and Informatics, Konan University, Higashinada-ku, Kobe 658-8501, Hyogo, Japan
9 Beyond5G Donated Lectures, Konan University, Higashinada-ku, Kobe 658-8501, Hyogo, Japan
* Correspondence: kayamori@konan-u.ac.jp (F.K.); kusui@konan-u.ac.jp (K.U.)

Abstract: Microwave applications, such as microwave ovens and mobile phones, are ubiquitous and indispensable in modern society. As the utilization of microwave technology is becoming more widespread, the effects of microwaves on living organisms and physiological processes have received increased attention. This study aimed to investigate the effects of microwaves on calcium carbonate biomineralization as a model biochemical process. A magnetron oscillator was used to generate 2450 MHz microwaves because magnetrons are relatively inexpensive and widespread. We conducted transmission electron microscopy (TEM), atomic force microscopy (AFM), TEM-electron energy-loss spectroscopy (EELS), dynamic light scattering (DLS), and high-performance liquid chromatography (HPLC) measurements to analyze the calcium carbonate precipitates. Our findings showed the formation of string-like precipitates of calcium carbonate upon microwave irradiation from one direction, similar to those obtained using a semiconductor oscillator, as reported previously. This implied that the distribution of the frequency had little effect on the morphology. Furthermore, spherical precipitates were obtained upon microwave irradiation from two directions, indicating that the morphology could be controlled by varying the direction of microwave irradiation. Magnetrons are versatile and also used in large-scale production; thus, this method has potential in medical and industrial applications.

Keywords: $CaCO_3$ mineralization; peptide; microwave; magnetron oscillator; irradiation direction

Citation: Kayamori, F.; Togashi, H.; Endo, N.; Ozaki, M.; Hirao, K.; Arimoto, Y.; Osawa, R.; Tsuruoka, T.; Imai, T.; Tomizaki, K.-y.; et al. Development of a $CaCO_3$ Precipitation Method Using a Peptide and Microwaves Generated by a Magnetron. *Processes* **2024**, *12*, 1327. https://doi.org/10.3390/pr12071327

Academic Editor: Krist V. Gernaey

Received: 25 March 2024
Revised: 24 April 2024
Accepted: 21 June 2024
Published: 26 June 2024

1. Introduction

Microwave (MW) applications such as MW ovens and mobile phones are ubiquitous and indispensable in modern society. In the field of chemistry, MWs are used to synthesize inorganic compounds [1–4] as well as organic compounds [5–11] including peptides [12,13]. With the increasingly widespread utilization of the MW technology, the effects of MWs on living organisms and physiological processes are receiving increasing attention. Although the effects of MWs on physiological functions have been studied in the field of life science, the elucidation of the detailed mechanism of the MW effects is only at a nascent stage. For example, the effects of MWs on biomineralization were investigated for hydroxyapatite mineralization on the surface of polydopamine nanospheres without biomolecules, and it

was reported that the formation of the precipitates was promoted by MWs [14]. Physiological functions are generally regulated through complex interactions between biomolecules such as peptides and proteins. Thus, detailed analyses of the behavior of these biomolecules under MW irradiation are needed. This study aimed to investigate calcium carbonate ($CaCO_3$) biomineralization—a process by which crustacean exoskeletons are formed—as a model biochemical process [15–25]. We recently reported the effect of MWs generated by a semiconductor oscillator that outputted a narrow frequency band of 2450 ± 3 MHz on $CaCO_3$ mineralization using peptides with different net charges. Our results showed that the nanomorphology of the $CaCO_3$ precipitates was dependent on the MW output (10–60 W) and the ability of the peptide to induce $CaCO_3$ precipitation [26]. Investigating the effects of MWs on the $CaCO_3$ mineralization with peptides enabled the elucidation of the molecular behavior of organic and inorganic compounds. In this study, we used a magnetron oscillator with a wider frequency band of 2450 ± 50 MHz, which is often used in daily life, and determined whether a similar morphological change occurred. Additionally, we analyzed the correlation between the irradiation conditions, such as the irradiation direction of the MWs (10–200 W) and electric field (E-field) strength, and the morphology, particle size, and peptide consumption rate upon mineralization. Our results revealed that the morphology could be controlled by varying the direction of MW irradiation. Although the frequency and output of the MWs generated by a magnetron are not as stable as those generated by a semiconductor oscillator, magnetrons are relatively inexpensive and are used in large-scale production. Thus, this method holds potential for medical and industrial applications.

2. Materials and Methods

2.1. Materials

All chemicals and solvents were of a reagent or HPLC grade and used without further purification. Amino acid monomers *N*-α-Fmoc-L-aspartic acid β-*t*-butyl ester (Fmoc-Asp(O*t*Bu)-OH), *N*-α-Fmoc-L-glutamic acid γ-*t*-butyl ester (Fmoc-Glu(O*t*Bu)-OH), and *N*-α-Fmoc-*O*-*t*-butyl-L-serine (Fmoc-Ser(*t*Bu)-OH) were used. The amino acids, Wang resin, *N*,*N*′-diisopropylcarbodiimide (DIPCI), 2-(1*H*-benzotriazole-1-yl)-1,1,3,3-tetramethyluronium hexafluorophosphate (HBTU), 1-hydroxy benzotriazole monohydrate (HOBt), *N*,*N*- diisopropylethylamine (DIEA), trifluoroacetic acid (TFA), and piperidine were purchased from Watanabe Chemical Industries, Ltd. (Watanabe, Hiroshima, Japan). *N*,*N*-Dimethyl-4-aminopyridine (DMAP) was purchased from Tokyo Chemical Industry Co., Ltd. (TCI, Tokyo, Japan). *N*-Methylpyrrolidone (NMP), triisopropylsilane, thioanisole, and diethyl ether were purchased from FUJIFILM Wako Pure Chemical Corporation (Wako, Osaka, Japan).

2.2. Peptide Synthesis

The peptide was manually synthesized. In order to obtain the peptide with a C-terminal carboxy group, Wang resin was used as a solid support, and coupling of the amino acid (10 eq.) was performed using DIPCI (5 eq.) and DMAP (0.1 eq.) for the first residue. For the subsequent residues, coupling of the amino acid (4 eq.) was performed using HBTU (4 eq.) and HOBt (4 eq.) in the presence of DIEA (8 eq.) by the Fmoc solid-phase synthesis method [27]. The deprotection of the Fmoc group was performed with 25% piperidine and 1% HOBt in NMP to prevent the formation of aspartimide. The obtained peptidyl resins were washed five times with chloroform and dried in vacuo. Cleavage of the synthesized peptide from the resin and removal of the protecting groups in the side chain were conducted by treatment with TFA/H_2O/triisopropylsilane/thioanisole (50/1/1/1, *v*/*v*) for 1 h. The peptide was precipitated by adding cold diethyl ether, collected by centrifugation, and dried in vacuo. Crude peptides were purified by reversed-phase high-performance liquid chromatography (RP-HPLC). RP-HPLC was conducted on a GL7410 HPLC system (GL Sciences Inc., Tokyo, Japan) with an Inertsil ODS-3 column (10 × 250 mm; GL Sciences) for preparative purification using a 0.1% TFA/Milli-Q water solution (A solution) and 0.08% TFA/acetonitrile solution (B solution). The elution was conducted using a linear gradient from 0% to 30% of the B solution over 30 min at a

flow rate of 3.0 mL/min. The purified peptide was characterized by matrix-assisted laser desorption/ionization time-of-flight mass spectrometry (MALDI-TOF MS) using an Autoflex III (Bruker Daltonics Inc., Billerrica, MA, USA) mass spectrometer: m/z 1012.8 ($[M+H]^+$ calcd. 1012.8). The peptide was dissolved in Milli-Q water at a concentration of ~1 mM, and peptide concentration was determined by an amino acid analysis. The amino acid analysis was performed with an Inertsil ODS-2 column (4.6 × 200 mm; GL Sciences) after hydrolyzing the peptide in 6 M HCl at 110 °C for 24 h, followed by labeling with phenylisothiocyanate.

2.3. MW Irradiation Equipment

The MW irradiation equipment using a magnetron oscillator was manufactured as a medical apparatus by Minato Medical Science Co., Ltd., Osaka, Japan. The MW output was 10–200 W (10 W steps), and the frequency was 2450 ± 50 MHz. The power was output to an AC transformer-type system, and a patch antenna (linearly polarized wave) with a voltage standing-wave ratio (VSWR) of < 1.4 was used. The MW generator was connected with a coaxial waveguide converter, and the MW power loss was corrected in advance. MW irradiation was performed as follows: (1) the MW irradiation for 80 min, (2) termination of MW irradiation and subsequent incubation for 20 min at room temperature, and (3) MW irradiation for 80 min. MW irradiation from two directions was performed alternately using two patch antennas at intervals of 8 ms with a phase difference of 180°.

2.4. Measurements of E-Fields' Strength

The E-fields generated by MW irradiating equipment were monitored with a controller (C3-1055, Seikoh Giken Co., Ltd., Matsudo, Japan) and a sensor head (6 × 6 × 23 mm, CS-1403, Seikoh Giken Co., Ltd., Matsudo, Japan). The E-field strength [dBμV/m] was calculated using the following formula:

$$E\ [dB\mu V/m] = P\ [dBm] + AF\ [dB/m] + 107$$

Here, P is the controller output [dBm], and AF is the antenna factor [dB/m].

2.5. Measurements of Sample Temperature

A thermocouple thermometer (Card Logger MR5300, MR9302, CHINO Corp., Tokyo, Japan) was used to measure the temperature changes in Milli-Q water (1 mL) in a microtube upon MW irradiation from one direction at 10, 30, and 200 W or from two directions at 10 and 200 W. In the previous study, we already confirmed that the effect of MWs on the thermometer was negligible [26].

2.6. $CaCO_3$ Mineralization in the Presence and Absence of MW Irradiation

Prior to $CaCO_3$ mineralization, 0.5 mmol of $CaCO_3$ was suspended in 30 mL of Milli-Q water. CO_2 was bubbled into the suspension for 1 h and then the residual solid $CaCO_3$ was filtered off. The Ca^{2+} concentration in the $Ca(HCO_3)_2$ solution was determined by titration using ethylenediaminetetraacetate. The concentration of $Ca(HCO_3)_2$ and the peptide was adjusted to 150 and 100 μM with Milli-Q water, respectively, in a microtube, and afterwards $CaCO_3$ mineralization was performed for 180 min. MW irradiation was conducted as follows: (1) the MW irradiation for 80 min, (2) termination of MW irradiation and subsequent incubation for 20 min at room temperature, and (3) MW irradiation for 80 min. To realize MW irradiation from two directions, MWs were irradiated alternately using two patch antennas at intervals of 8 ms with a phase difference of 180°. In the absence of MW irradiation, incubation was performed at 30, 50, 60, and 90 °C using a temperature control device (GeneAtlas 485, ASTEC Co., Ltd., Fukuoka, Japan).

2.7. TEM and TEM-EELS Measurements

A 20 μL solution of the $CaCO_3$ precipitates was placed on a transmission electron microscopy (TEM) grid for 5 min, and the excess solvent was absorbed with filter paper;

this process was repeated. Milli-Q water (20 μL) was placed on the grid and immediately absorbed with a filter paper. All samples were dried in vacuo prior to the TEM measurements, which were conducted at an accelerating voltage of 200 kV (JEM-2100, JEOL Ltd., Tokyo, Japan).

2.8. AFM Measurements

A 20 μL solution of the $CaCO_3$ precipitates was placed on freshly cleaved mica (1 × 1 cm) for 5 min and the excess solvent was absorbed with filter paper. This process was repeated, and afterwards 20 μL of Milli-Q water was placed on the mica surface and immediately absorbed with a filter paper. All samples were dried in vacuo. Tapping-mode images were obtained on a multimode scanning probe microscope using a Nanoscope IIIa controller (Veeco Instruments Inc., Woodbury, NY, USA).

2.9. DLS Measurements

An 80 μL solution of the $CaCO_3$ precipitates was transferred into a cuvette (ZEN0040, Malvern Panalytical Ltd., Malvern, UK) for the dynamic light scattering (DLS) measurements. DLS data were obtained on a Zetasizer ZEN3600 instrument (Sysmex Corp., Kobe, Japan).

2.10. HPLC Analysis for Peptide Consumption Rates

Following the $CaCO_3$ mineralization, 100 μM peptide, 150 μM $Ca(HCO_3)_2$, and 0.1% TFA/Milli-Q water (40 μL) were added to 160 μL of the sample solution. Then, 200 μL of the solution was filtered using a centrifugal filter (Durapore®-PVDF 0.45 μm Ultrafree®-MC-HV, Merck KGaA, Tokyo, Japan). The sample (150 μL) was analyzed using an Inertsil ODS-3 column (4.6 × 150 mm; GL Science). The sample was eluted with A and B solutions using a linear gradient from 0% to 30% of the B solution over 30 min at a flow rate of 1.0 mL/min. HPLC analyses were performed on the sample after $CaCO_3$ mineralization using 100 μM peptide. The peptide consumption rates (ratio of the peptide content trapped in or bound to the $CaCO_3$ precipitates to the initial peptide content) were estimated from the HPLC peak area of the unreacted peptide (i.e., the remaining peptide) (Figure S1).

3. Results and Discussion

3.1. Design of the $CaCO_3$-Precipitating Peptide

The effects of MWs on $CaCO_3$ mineralization were previously investigated using four peptides that had different net charges owing to structural modification at the *C*-terminal core sequence of the calcification-associated peptide (CAP-1) [15]. We showed that MWs generated from a semiconductor oscillator altered the nanomorphology of the $CaCO_3$ precipitates [26]. MWs barely affected the morphology of the $CaCO_3$ precipitates when using the peptide with high mineralization ability, whereas they significantly affected the precipitate morphology when using the peptide with low mineralization ability. In this study, among the four peptides, we selected the peptide that exhibited the lowest precipitating ability and large MW effect (Figure 1). When the selected $CaCO_3$-precipitating peptide was used at a concentration of 100 μM, the $CaCO_3$ precipitates showed string-like morphology upon irradiation with 60 W of MWs generated by the semiconductor oscillator [26].

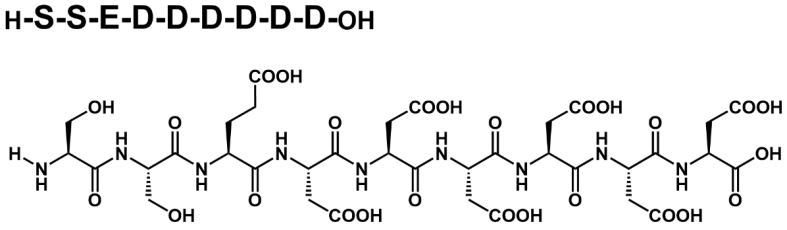

Figure 1. Sequence and structure of $CaCO_3$-precipitating peptide.

3.2. Development of the MW Irradiating Equipment

We used a magnetron as an MW oscillator and placed an antenna below the sample in a microtube (Figure 2a). We analyzed the strength of the E-field generated by the MW irradiating equipment and monitored the polarizing direction. The distribution of the E-field strength was non-uniform, thus necessitating that the device measuring the E-field strength had a spatial resolution equal to or less than the microtube size. We used an optical E-field sensor that was composed of an optical waveguide and a dipole antenna, similar to that used in the previous study [26]. The E-field strength increased with the MW output (Figure S2), and the polarizing direction was vertical to the antenna major axis. This indicated that the equipment could generate an E-field with linear polarization, enabling us to analyze the behavior of the biomolecules upon MW irradiation in detail.

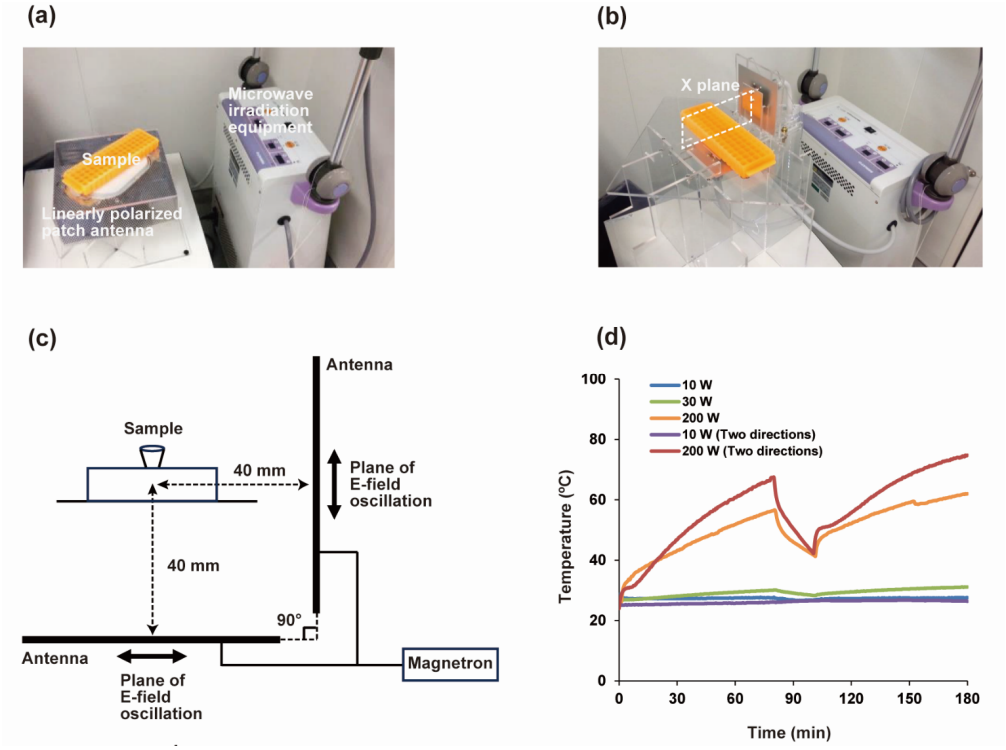

Figure 2. Equipment for MW irradiation. (**a**) Equipment for MW irradiation from one direction. (**b**) Equipment for MW irradiation from two directions. (**c**) The cross-sectional view of the irradiation equipment from the two directions along the X plane in (**b**). (**d**) The temperature variation of the solution upon changing the MW output. (**a**–**c**) were modified and reproduced from [28] with permission from the Japan Society of Electromagnetic Wave Energy Applications.

We next developed the MW irradiation equipment so as to realize irradiation from two directions (Figure 2b). First, we divided the MWs generated by the magnetron into two parts and attempted to irradiate the MWs from the two antennas simultaneously. However, the magnetron was saturated by the MWs, which leaked from the sides of the antenna, failing to generate MWs at the expected output. Therefore, the MWs were irradiated alternately from two patch antennas to suppress the saturation of the magnetron. Two patch antennas were installed at an angle of 90° such that the planes of the polarization of the linearly polarized waves intersected at right angles (Figure 2c) and the MW irradiation could be performed alternately at intervals of 8 ms with a phase difference of 180° to prevent interference.

Next, the sample solution temperature was measured using a thermocouple thermometer under MW irradiation. The maximum and average temperature gradually increased with the MW output. For MW irradiation from one direction at 200 W, the maximum and

average temperatures of the sample solution were 62.3 and 50.5 °C, respectively. For MW irradiation from two directions at 200 W, the maximum and average temperatures were 74.8 and 56.2 °C, respectively (Figure 2d).

3.3. Morphology of the $CaCO_3$ Precipitates Formed by MW Irradiation from One Direction

We observed the $CaCO_3$ precipitates obtained using 100 μM peptide in the presence and absence of MW irradiation. TEM images showed sphere-like precipitates of $CaCO_3$ in the absence of MW irradiation at room temperature, 30, 50, 60, and 90 °C (Figure 3a and Figure S3a–d). Considering the local heating by MWs, we performed the $CaCO_3$ mineralization at 90 °C in the absence of MW irradiation. Under MW irradiation, string-like precipitates were formed (Figures 3b and S3e,f). On the other hand, in the absence of the peptide, the string-like precipitates were barely formed even under MW irradiation at 200 W (Figure S3h). In the atomic force microscopy (AFM) images, spherical $CaCO_3$ precipitates were observed in the absence of MW irradiation at room temperature, 50, and 60 °C (Figure S4a–c), and string-like precipitates were observed upon MW irradiation (Figure S4d,e). This was consistent with the TEM analysis. These results showed that the string-like precipitates of $CaCO_3$ were formed upon MW irradiation from the one direction, similar to that observed using the semiconductor oscillator described previously. The magnetron oscillator outputted a wide frequency band of 2450 ± 50 MHz, whereas the semiconductor oscillator outputted a narrower frequency band of 2450 ± 3 MHz. These observations suggest that the distribution of the MW frequency has a negligible effect on the morphology.

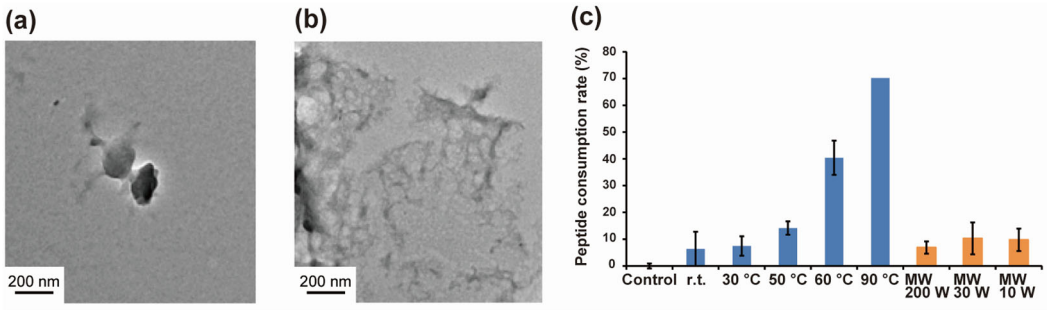

Figure 3. $CaCO_3$ precipitates formed under MW irradiation from one direction and consumption rate of peptides on $CaCO_3$ mineralization. (**a**) TEM image of $CaCO_3$ precipitates with 100 μM peptide at 60 °C without MW irradiation (representative of sphere-like image). (**b**) TEM image of $CaCO_3$ precipitates with 100 μM peptide under 200 W MW irradiation (representative of string-like image). (**c**) Peptide consumption rates calculated from peak areas of residual peptides determined in HPLC profiles.

Next, we conducted the elemental analysis of the $CaCO_3$ precipitates obtained using the peptide in the presence and absence of MW irradiation by TEM-electron energy-loss spectroscopy (TEM-EELS). Calcium from $CaCO_3$, nitrogen from the peptide, and oxygen from $CaCO_3$ and/or the peptide were slightly detected (Figure S5), indicating that the precipitates observed in the TEM images were those of $CaCO_3$ and peptides.

We then determined the size distribution profile of the $CaCO_3$ precipitates obtained using 100 μM peptide in the presence and absence of MW irradiation by DLS measurements. A single peak (corresponding to 1 mm particle size) was observed in the absence of MW irradiation at 50 and 60 °C, while two peaks (corresponding to particle sizes of 200 nm and 1 mm) were observed under MW irradiation at 200 W; these two peaks were correlated to the morphology observed in the TEM images. These results indicated that different precipitates of $CaCO_3$ were formed with or without MW irradiation.

Finally, the peptide consumption rates (ratio of the peptide content trapped in or bound to $CaCO_3$ precipitates to the initial peptide content) were estimated with HPLC (Figure 3c). The peptide consumption rates increased with temperature in the absence of

MW irradiation, whereas they remained almost unchanged regardless of the MW output under MW irradiation. Therefore, MWs have lesser effect on the peptide.

MWs can generate local hot spots at the contact points of particles [29]. Thus, we assume that once a peptide precipitates the $CaCO_3$ nanoparticles, linearly polarized MWs can create an anisotropic E-field and induce thermal distribution in the nanoparticles. Considering this, we speculated that in the presence of peptides, the hotspots generated between the particles accelerated the $CaCO_3$ precipitation to form string-like $CaCO_3$ precipitates under MW irradiation from one direction.

3.4. Morphology of $CaCO_3$ Precipitates Formed under MW Irradiation from Two Directions

We investigated the effect of the irradiation direction of the MWs on the $CaCO_3$ mineralization using the peptide. The TEM images showed the formation of $CaCO_3$ precipitates with sphere-like shapes under MW irradiation from two directions at 10 and 200 W (Figures 4a,b and S6). This was similar to that observed at 60 °C in the absence of MW irradiation (Figure 3a), but different from the string-like $CaCO_3$ precipitates formed under MW irradiation from one direction. These results indicated that the direction of MW irradiation strongly affected the $CaCO_3$ morphology.

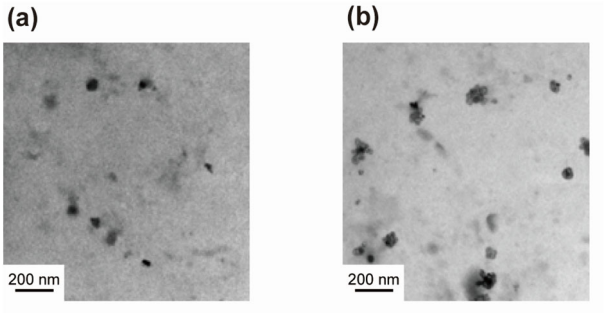

Figure 4. TEM images of $CaCO_3$ precipitates obtained under MW irradiation from two directions. $CaCO_3$ mineralization using 100 μM peptide was performed under MW irradiation at (**a**) 10 W and (**b**) 200 W (both representative of sphere-like particles).

Considering this, we speculated that the E-field and thermal distribution were not anisotropic under MW irradiation from two directions, and thus sphere-like $CaCO_3$ precipitates were formed.

4. Conclusions

In conclusion, the irradiation direction of the MWs generated by the magnetron affected the morphology of the $CaCO_3$ precipitates. String-like $CaCO_3$ precipitates were formed under MW irradiation from one direction, similar to those obtained using a semiconductor oscillator described previously. This implied that the distribution of the frequency had a negligible effect on the morphology. In contrast, spherical precipitates were obtained under MW irradiation from two directions. Thus, we developed a method to control the morphology of the $CaCO_3$ precipitates by varying the direction of MW irradiation. In the future, we plan to analyze the polymorphism of the $CaCO_3$ precipitates obtained under MW irradiation. Mineralization through MW irradiation is not limited to the production of $CaCO_3$ precipitates. By substituting the $CaCO_3$-precipitating sequences with other inorganic compound-precipitating sequences, this system can be used to obtain various inorganic compound precipitates with controlled shapes. Mineralization through MW irradiation can be applied not only to the industrial production of inorganic materials but also for the treatment of teeth and bones. Magnetrons are relatively inexpensive and versatile, and thus mineralization using the MWs generated by magnetrons has potential for widespread application. We shall investigate the effects of MWs with stronger E-field strength on the $CaCO_3$ mineralization for industrial and medical applications.

Supplementary Materials: The following supporting information can be downloaded at: https://www.mdpi.com/article/10.3390/pr12071327/s1, Figure S1: Example of HPLC charts for analyzing peptide consumed in $CaCO_3$ mineralization; Figure S2: Relationships between output power of the one-direction linearly polarized irradiation system and the E-field strength around the sample; Figure S3: TEM images of the sample after $CaCO_3$ mineralization using 100 μM peptide; Figure S4: AFM images of the sample after $CaCO_3$ mineralization using 100 μM peptide; Figure S5: TEM-EELS measurement of the sample after $CaCO_3$ mineralization using the peptide; Figure S6: TEM images of the sample after $CaCO_3$ mineralization under MW irradiation from two directions.

Author Contributions: Conceptualization, H.T., T.U., N.N. and K.U.; methodology, F.K., H.T., M.O., Y.A., R.O., T.T., T.I., K.-y.T., T.U. and N.N.; investigation, N.E., M.O., K.H., R.O. and T.I.; writing—original draft preparation, F.K. and K.U.; visualization, F.K. and K.U.; writing—review and editing, F.K., K.-y.T. and K.U. All authors have read and agreed to the published version of the manuscript.

Funding: This study (for F.K. and K.U.) was supported in part by the JST CREST (JPMJCR21B2).

Data Availability Statement: The data presented in this study are available on request from the corresponding author.

Acknowledgments: The authors thank K. Akamatsu (Konan University, Kobe, Japan), K. Minaki (DSP Research, Inc., Kobe, Japan), and T. Uraka (Minato Medical Science Co., Ltd., Osaka, Japan) for valuable discussions and generous support.

Conflicts of Interest: Authors Hiroyuki Togashi and Nobuhiro Nakanishi were employed by the DSP Research, Inc. Yonejiro Arimoto was employed by the Minato Medical Science Co., Ltd. Ryuji Osawa was employed by the Seikoh Giken Co., Ltd. The remaining authors declare that the research was conducted in the absence of any commercial or financial relationships that could be construed as a potential conflict of interest. The companies had no role in the design of the study; in the collection, analyses, or interpretation of data; in the writing of the manuscript, or in the decision to publish the results.

References

1. Kitchen, H.J.; Vallance, S.R.; Kennedy, J.L.; Tapia-Ruiz, N.; Carassiti, L.; Harrison, A.; Whittaker, A.G.; Drysdale, T.D.; Kingman, S.W.; Gregory, D.H. Modern microwave methods in solid-state inorganic materials chemistry: From fundamentals to manufacturing. *Chem. Rev.* **2014**, *114*, 1170–1206. [CrossRef] [PubMed]
2. Zhu, Y.-J.; Chen, F. Microwave-assisted preparation of inorganic nanostructures in liquid phase. *Chem. Rev.* **2014**, *114*, 6462–6555. [CrossRef] [PubMed]
3. Wojnarowicz, J.; Chudoba, T.; Lojkowski, W. A review of microwave synthesis of zinc oxide nanomaterials: Reactants, process parameters and morphologies. *Nanomaterials* **2020**, *10*, 1086. [CrossRef] [PubMed]
4. Salvatore, K.L.; Deng, K.; McGuire, S.C.; Tan, S.; Rui, N.; Zhang, L.; Rodriguez, J.A.; Wong, S.S. Microwave-assisted synthesis of $Cu@IrO_2$ core-shell nanowires for low-temperature methane conversion. *ACS Appl. Nano Mater.* **2021**, *4*, 11145–11158. [CrossRef]
5. De la Hoz, A.; Díaz-Ortiza, Á.; Moreno, A. Microwaves in organic synthesis. Thermal and non-thermal microwave effects. *Chem. Soc. Rev.* **2005**, *34*, 164–178. [CrossRef] [PubMed]
6. Rahman, M.; Ghosh, S.; Bhattacherjee, D.; Zyryanov, G.V.; Bagdi, A.K.; Hajra, A. Recent advances in microwave-assisted cross-coupling reactions. *Asian J. Chem.* **2022**, *11*, e202200179. [CrossRef]
7. Tsukahara, Y.; Higashi, A.; Yamauchi, T.; Nakamura, T.; Yasuda, M.; Baba, A.; Wada, Y. In situ observation of nonequilibrium local heating as an origin of special effect of microwave on chemistry. *J. Phys. Chem. C* **2010**, *114*, 8965–8970. [CrossRef]
8. Horikoshi, S.; Watanabe, T.; Narita, A.; Suzuki, Y.; Serpone, N. The electromagnetic wave energy effect(s) in microwave-assisted organic syntheses (MAOS). *Sci. Rep.* **2018**, *8*, 5151. [CrossRef]
9. Frasso, M.A.; Stiegman, A.E.; Dudley, G.B. Microwave-specific acceleration of a retro-Diels-Alder reaction. *Chem. Commun.* **2021**, *56*, 11247–11250. [CrossRef]
10. Yamada, M.; Ohta, R.; Harada, K.; Takehara, T.; Haneoka, H.; Murakami, Y.; Suzuki, T.; Ohki, Y.; Takahashi, N.; Akiyama, T.; et al. Product selective reaction controlled by the combination of palladium nanoparticles, continuous microwave irradiation, and a co-existing solid; ligand-free Buchwald-Hartwig amination vs. aryne amination. *Green Chem.* **2021**, *23*, 8131–8137. [CrossRef]
11. Matsukawa, Y.; Muranaka, A.; Murayama, T.; Uchiyama, M.; Takaya, H.; Yamada, Y.M.A. Microwave-assisted photooxidation of sulfoxides. *Sci. Rep.* **2021**, *11*, 20505. [CrossRef] [PubMed]
12. Pedersen, S.L.; Tofteng, A.P.; Malik, L.; Jensen, K.J. Microwave heating in solid-phase peptide synthesis. *Chem. Soc. Rev.* **2012**, *41*, 1826–1844. [CrossRef] [PubMed]
13. Hojo, K.; Manabe, Y.; Uda, T.; Tsuda, Y. Water-based solid-phase peptide synthesis without hydroxy side chain protection. *J. Org. Chem.* **2022**, *87*, 11362–11368. [CrossRef] [PubMed]

14. Ghorbani, F.; Zamanian, A.; Behnamghader, A.; Daliri-Joupari, M. Bone-like hydroxyapatite mineralization on the bio-inspired PDA nanoparticles using microwave irradiation. *Surf. Interfaces* **2019**, *15*, 38–42. [CrossRef]
15. Sugawara, A.; Nishimura, T.; Yamamoto, Y.; Inoue, H.; Nagasawa, H.; Kato, T. Self-organization of oriented calcium carbonate/polymer composites: Effects of a matrix peptide isolated from the exoskeleton of a crayfish. *Angew. Chem. Int. Ed.* **2006**, *45*, 2876–2879. [CrossRef] [PubMed]
16. Kumagai, H.; Matsunaga, R.; Nishimura, T.; Yamamoto, Y.; Kajiyama, S.; Oaki, Y.; Akaiwa, K.; Inoue, H.; Nagasawa, H.; Tsumoto, K.; et al. $CaCO_3$/Chitin hybrids: Recombinant acidic peptides based on a peptide extracted from the exoskeleton of a crayfish controls the structures of the hybrids. *Faraday Discuss.* **2012**, *159*, 483–494. [CrossRef]
17. Arakaki, A.; Shimizu, K.; Oda, M.; Sakamoto, T.; Nishimura, T.; Kato, T. Biomineralization-inspired synthesis of functional organic/inorganic hybrid materials: Organic molecular control of self-organization of hybrids. *Org. Biomol. Chem.* **2015**, *13*, 974–989. [CrossRef] [PubMed]
18. Lakshminarayanan, R.; Chi-Jin, E.O.; Loh, X.J.; Kini, R.M.; Valiyaveettil, S. Purification and characterization of a vaterite-inducing peptide, pelovaterin, from the eggshells of pelodiscus sinensis (Chinese soft-shelled turtle). *Biomacromolecules* **2005**, *6*, 1429–1437. [CrossRef] [PubMed]
19. Murai, K.; Kinoshita, T.; Nagata, K.; Higuchi, M. Mineralization of calcium carbonate on multifunctional peptide assembly acting as mineral source supplier and template. *Langmuir* **2016**, *32*, 9351–9359. [CrossRef] [PubMed]
20. Zhu, W.; Lin, J.; Cai, C. The effect of a thermo-responsive polypeptide-based copolymer on the mineralization of calcium carbonate. *J. Mater. Chem.* **2012**, *22*, 3939–3947. [CrossRef]
21. Elhadj, S.; Salter, E.A.; Wierzbicki, A.; De Yoreo, J.J.; Han, N.; Dove, P.M. Peptide controls on calcite mineralization: Polyaspartate chain length affects growth kinetics and acts as a stereochemical switch on morphology. *Cryst. Growth Des.* **2006**, *6*, 197–201. [CrossRef]
22. Usui, K.; Ozaki, M.; Yamada, A.; Hamada, Y.; Tsuruoka, T.; Imai, T.; Tomizaki, K. Site-specific control of multiple mineralizations using a designed peptide and DNA. *Nanoscale* **2016**, *8*, 17081–17084. [CrossRef] [PubMed]
23. Usui, K.; Yokota, S.; Ozaki, M.; Sakashita, S.; Imai, T.; Tomizaki, K. Modification of the N-terminus of a calcium carbonate precipitating peptide affects calcium carbonate mineralization. *Protein Pept. Lett.* **2018**, *25*, 42–47. [CrossRef] [PubMed]
24. Knight, B.M.; Edgar, K.J.; Yoreo, J.D.; Dove, P.M. Chitosan as a canvas for studies of macromolecular controls on $CaCO_3$ biological crystallization. *Biomacromolecules* **2023**, *24*, 1078–1102. [CrossRef] [PubMed]
25. Palmer, L.C.; Newcomb, C.J.; Kaltz, S.R.; Spoerke, E.D.; Stupp, S.I. Biomimetic systems for hydroxyapatite mineralization inspired by bone and enamel. *Chem. Rev.* **2008**, *108*, 4754–4783. [CrossRef] [PubMed]
26. Usui, K.; Ozaki, M.; Hirao, K.; Kosaka, T.; Endo, N.; Yoshida, S.; Yokota, S.; Arimoto, Y.; Osawa, R.; Nakanishi, N.; et al. Effect of linearly polarized microwaves on nanomorphology of calcium carbonate mineralization using peptides. *Sci. Rep.* **2023**, *13*, 12027. [CrossRef] [PubMed]
27. Chan, W.C.; White, P.D. *Fmoc Solid Phase Peptide Synthesis*; Oxford University Press: New York, NY, USA, 2000.
28. Usui, K.; Togashi, H.; Endo, N.; Ozaki, M.; Arimoto, Y.; Uraka, T.; Osawa, R.; Minaki, K.; Nakanishi, N.; Umetani, T. Microwave irradiation systems for analyses of biomolecular behaviors. *J. Jpn. Soc. Electromagn. Wave Energy Appl.* **2017**, *1*, 17–24. (In Japanese)
29. Tsubaki, S.; Matsuzawa, T.; Higuchi, T.; Fujii, S.; Wada, Y. Determining the influence of microwave-induced thermal unevenness on vanadium oxide catalyst particles. *Chem. Eng. J.* **2022**, *433*, 133603. [CrossRef]